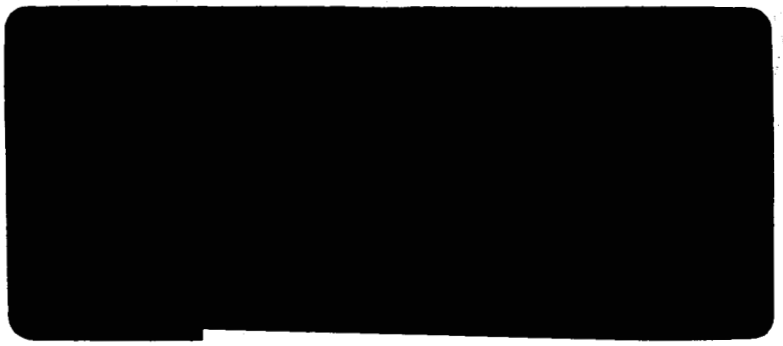

GPO PRICE $ _____

CFSTI PRICE(S) $ _____

Hard copy (HC) $3.00

Microfiche (MF) .50

ff 653 July 65

FACILITY FORM 602

N66-19136
(ACCESSION NUMBER) (THRU)

36 1
(PAGES) (CODE)

CR 70348 33
(NASA CR OR TMX OR AD NUMBER) (CATEGORY)

JET PROPULSION LABORATORY
CALIFORNIA INSTITUTE OF TECHNOLOGY
PASADENA, CALIFORNIA

CASE FILE COPY

Ref 3564

Technical Memorandum No. 33-175

The Effect of Solar Simulator Operating Characteristics on Spacecraft Thermal Tests

L. B. Katter

M. E. Kahn

M. G. Comuntzis

M. G. Comuntzis, *Chief*
Spacecraft Design

JET PROPULSION LABORATORY
CALIFORNIA INSTITUTE OF TECHNOLOGY
PASADENA, CALIFORNIA

July 15, 1964

Prepared Under Contract No. NAS 7-100
National Aeronautics & Space Administration

CONTENTS

TABLES

TABLES (Cont'd)

FIGURES

PREFACE

The original work on this report was done by L.B. Katter before he left JPL in December 1962. At that time, the *Ranger* Block II program was essentially completed. The temperature control design of the *Ranger* Block III spacecraft had not been completed. For this reason, most of the numerical values for power dissipation, surface properties, etc., used for calculations in the original draft of the report, reflected the thermal design of the *Ranger* Block II spacecraft. When work was resumed on the report, it was decided to leave the numerical calculations as they were and to supplement them with an appendix reflecting the *Ranger* Block III thermal design. The revised calculations are contained in Appendix A.

Since the completion of the *Ranger* Block II program, four thermal tests with solar simulation have been performed in the JPL 25-ft Space Simulator by the *Ranger* temperature control group. In Appendix B, some comments are made relative to problems encountered in performing these tests and analyzing the results.

Technical Memorandum No. 33-175

The Effect of Solar Simulator Operating Characteristics on Spacecraft Thermal Tests

L. B. Katter
M. E. Kahn

JET PROPULSION LABORATORY
CALIFORNIA INSTITUTE OF TECHNOLOGY
PASADENA, CALIFORNIA

July 15, 1964

ABSTRACT

19136

A study has been made to determine the effect of various solar simulator operating characteristics on spacecraft thermal tests. Characteristics considered are: (1) the effects of decollimation, (2) spectral mismatch, and (3) axial and radial variations of energy flux density. In addition, the effect of solar simulator optics in the chamber has been considered for certain special cases.

Author

I. INTRODUCTION

At the present time, spacecraft thermal control design is based primarily on analysis. Practicality limits the number of pieces into which the spacecraft can be separated for analysis and the degree of detail with which these individual pieces of the spacecraft may be analyzed. The capability of handling more of this analysis by computer techniques is being developed. However, the uncertainties in solar absorptance, emittance, joint conductance, and internal power dissipation, coupled with the difficulty of calculating combined specular and diffuse heat transfer, limit the solutions to the prediction of a relatively wide span for steady-state flight temperatures and transient temperatures. A *valid* experimental verification of the analytically determined thermal design is highly desirable and could result in a reduction in the required operating temperature range for many of the spacecraft electronic components, thus increasing spacecraft reliability.

For any constant temperature portion of a spacecraft (node) radiating to space at steady state, the temperature of the node will be defined by the statement of energy conservation

$$\Sigma q_n = A \bar{\epsilon} \sigma T^4 \tag{1}$$

where

Σq_n = net heat input to the node

A = the external radiating area of the node

$\bar{\epsilon}$ = the average emittance of the node

T = the absolute temperature of the node

σ = the Stephan-Boltzmann constant

Taking the logarithm and then the differential of Eq. (1) gives

$$\frac{\Delta \Sigma q_n}{\Sigma q_n} = \frac{\Delta A}{A} + \frac{\Delta \bar{\epsilon}}{\bar{\epsilon}} + 4\frac{\Delta T}{T} \tag{2}$$

Assuming that the external area is known (or can be measured) with negligible error ($\Delta A \approx 0$), Eq. (2) reduces to

$$\frac{\Delta \Sigma q_n}{\Sigma q_n} = \frac{\Delta \bar{\epsilon}}{\bar{\epsilon}} + 4\frac{\Delta T}{T} \tag{3}$$

The conservative assumption that the errors in the individual terms making up Eq. (3) should be added in a scalar manner rather than statistically yields

$$\frac{\Sigma \Delta q_n}{\Sigma q_n} = \frac{\Delta \bar{\epsilon}}{\bar{\epsilon}} + 4\frac{\Delta T}{T} \tag{4}$$

This form of the statement of energy conservation will be useful for the discussion to follow.

The information of primary interest in analysis and thermal testing of a spacecraft is the temperature distribution among the various spacecraft nodes. Equation (4) may be rearranged to show the dependence of temperature deviation from nominal flight temperature on variation of emittance and net heat input to a node.

$$\frac{\Delta T}{T} = \frac{1}{4}\left[\frac{\Sigma \Delta q_n}{\Sigma q_n} - \frac{\Delta \bar{\epsilon}}{\bar{\epsilon}}\right] \tag{4'}$$

It can be seen that a decrease in emittance has the same effect on temperature as an increase in net heat input. Thus, the worst temperature deviation will occur when $\Sigma \Delta q_n / \Sigma q_n$ and $\Delta \bar{\epsilon} / \bar{\epsilon}$ are of opposite sign.

In appraising the value of solar simulator testing in relation to analysis, it is more convenient to examine the variations of heat input to a node rather than variations in temperature. An estimate of the error in the calculated heat input to a node may be obtained by evaluation of the terms on the right side of Eq. (4). This error may be compared with the estimated error in heat input during solar simulator testing.

II. HEAT INPUT ERROR IN ANALYSIS

The design operating temperature for most spacecraft electronics is 85 F, with an allowable temperature range of ± 13 F. In thermal design calculations, an attempt was made in the past to design to a temperature as close as possible to the design operating temperature or to the mean of the upper and lower temperature limits for a given node. As previously mentioned, these calculations result in a relatively wide span for steady-state flight temperatures and maneuver transient temperatures. Under worst case conditions, ΔT for the node could be as large as 13 F about a nominal 85 F during steady-state (cruise) operation.

Table 1 lists the emittances of six surface treatments used on the *Ranger* spacecraft. The uncertainties shown result from the resolving power of the instruments used to measure the emittances of the surfaces.

Table 1. Absolute emittance and relative uncertainty of typical spacecraft surfaces

Material	Absolute emittance	Relative uncertainty, %
Black paint	0.90 ± 0.02	2
White paint (PV 100)	0.85 ± 0.02	2
White paint (JW 40)	0.78 ± 0.02	3
Aluminum paint	0.30 ± 0.03	10
Polished aluminum (commercial polish)	0.045 ± 0.005	11
Gold plate	0.035 ± 0.005	14

The desired average emittance of the *Ranger* Block II spacecraft electronic assemblies fell between 0.1 and 0.3. These emittances were achieved by mosaics of white paint applied to gold plate or commercially polished aluminum. For this range of emittances, the unknown would be 11% to 4% respectively, with 6% representing the mid-range.

The variations of emittance and temperature associated with analytical design were discussed in the preceding paragraphs. These values may be used in Eq. (4) with the sign relationships discussed to obtain a numerical value for $\Sigma \Delta q_{in} \Sigma q_{in}$ under the condition of worst temperature deviation:

$$\frac{\Sigma \Delta q_n}{\Sigma q_n} = \mp 0.06 + 4\left(\pm \frac{43}{545}\right) = \pm 0.26 \tag{5}$$

Thus, if solar simulator testing is to provide a significant improvement over analysis, the total heat input to the node in question must be within ±26% of its flight value. The possible sources of errors in heat input during solar simulator testing will be discussed below.

III. SOURCES OF HEAT INPUT

In space, the sources of heat input to a spacecraft node are the following:

1. Electrical power dissipation.
2. Absorption of directly incident solar energy.
3. Absorption of indirectly incident (reflected) solar energy.
4. Intercepted infrared emission from other spacecraft parts.
5. Net conduction from other spacecraft parts.

During a vacuum thermal test with solar simulation, each of these five inputs will be simulated with some error. In addition to these inputs, some additional "un-space-like" inputs will occur during testing. These un-space-like inputs can be broken into the following classes:

6. Energy absorbed on surfaces parallel to the Sun – probe line due to decollimation of the solar simulator.
7. Energy reflected by the spacecraft back to the solar simulator and rereflected again to the spacecraft.
8. Energy emitted by the spacecraft and returned to the spacecraft in a manner similar to that of the preceding input.
9. Energy emitted by the various optical elements of the solar simulation system.
10. Energy reflected and emitted by the cold (−320°F) black wall shroud.

The errors associated with the above inputs to a subassembly may be compensating, accumulative, or negligible, depending strongly on the spacecraft configuration and on the geometry of the subassembly. A summation of the differences between the values of terms 1 – 5 in a solar simulator test and their respective counterparts in space and of the values of terms 6 – 9 will give a conservative value of $\Sigma \Delta q_n$. Input 10 will not be included in the summation since it is mainly a function of chamber geometry (which is not considered in this memorandum) and is relatively insensitive to the quality of solar simulation. The preceding summation may be divided by a summation of space inputs 1 – 5 to arrive at a value of $\Sigma \Delta q_n / \Sigma q_n$. Thus,

$$\frac{\Sigma \Delta q_n}{\Sigma q_n} = \frac{\Delta q_1 + \Delta q_2 + \Delta q_3 + \Delta q_4 + \Delta q_5 + \Delta q_6 + \Delta q_7 + \Delta q_8 + \Delta q_9}{q_1 + q_2 + q_3 + q_4 + q_5} \tag{6}$$

This summation may be compared with the value determined above in Eq. (5).

IV. TERM-BY-TERM DISCUSSION OF HEAT INPUTS

A. Electrical Power Dissipation, q_1

Sources of differences between electrical power dissipation in space and in a test chamber are non-flight hardware, ground-type power systems, and power through instrumentation cabling during these tests. A continuing effort to minimize these sources of error seems to have reduced them to a negligible magnitude. As for measurement of q_1, itself, we are not so well off. Measuring techniques and statistical variations of sub-components preclude an exact measurement of q_1. At this time most power measurements are thought to be accurate to ±5%. A typical set of power dissipations for the *Ranger* Block II spacecrafts is given in Table 2.

Table 2. Average power dissipation for three spacecraft elements, q_1

Object	Power dissipation, w
Major electronic assembly	4.4 to 26.4
Scientific package	0.03 to 0.88
Structure	0

B. Direct Solar Absorption, q_2

In space, 130 watts of solar energy per square foot of normal area is nominally incident at the Earth's mean distance from the Sun. The fraction of this energy (α) absorbed by a surface in space depends strongly on the surface properties and configuration with respect to the Sun. Table 3 shows the solar energy typically absorbed (q_2) by various *Ranger* objects during flight. During thermal vacuum tests with solar simulation, errors in "solar" energy absorbed will arise because of imperfect spectral match and imperfect collimation (decollimation) of the solar simulator. For purposes of analysis, it becomes convenient to separate these errors so that $\Delta q_2 = \Delta q_{2\ \text{spectral}} + \Delta q_{2\ \text{decollimation}}$. A discussion of each of these errors will follow.

The term $\Delta q_{2\ \text{spectral}}$ may be interpreted as the difference between the energy absorbed per unit normal area in space and that absorbed in a space simulator. The energy absorbed by a surface in space per unit normal area is given by the integral

$$q_2 = \int_0^\infty \alpha(\lambda)\, I_s(\lambda)\, d\lambda \tag{7}$$

Table 3. Solar energy absorbed by three spacecraft elements, q_2

Object	Solar energy absorbed, w
Major electronic assembly (average for 6 chassis, *Ranger* Block II)	9.7
Science assembly (*Ranger* Block I)	8.8 to 20.5
Structure (*Ranger* leg)	2.9

where

λ = wavelength

$\alpha(\lambda)$ = absorptance of material at wavelength λ

$I_s(\lambda)$ = flux density of solar radiant energy per unit area and unit wavelength at wavelength λ

In a solar simulator the energy absorbed per unit normal area is given by the integral

$$q_2' = \int_0^\infty \alpha(\lambda) \left[I_{ss}(\lambda) \rho_1(\lambda) \rho_2(\lambda) \cdots \rho_n(\lambda) \tau_1(\lambda) \tau_2(\lambda) \cdots \tau_n(\lambda) \right] d\lambda \tag{8}$$

where

λ = wavelength

$\alpha(\lambda)$ = absorptance of material at wavelength λ

$I_{ss}(\lambda)$ = flux density of solar simulator light source radiant energy per unit area and unit wavelength at wavelength λ

$\rho_n(\lambda)$ = reflectance of nth mirror element in optical system at wavelength λ

$\tau_n(\lambda)$ = transmittance of nth window or lens in optical system at wavelength λ

Notice that in Eq. (7) the energy absorbed is the integral of the product of the spectral absorptance and the spectral energy distribution of the source or Sun. Equation (8) has the same form as Eq. (7), the bracketed quantity being the effective spectral distribution of the solar simulation source in the test volume after having been modified by reflections and transmissions in the solar simulator optics. Thus, for a given surface [$\alpha(\lambda)$ fixed] the energy absorbed in various energy spectrums may vary greatly, depending on the spectral

characteristics of the source. The error $\Delta q_{2\ \text{spectral}}$ is the result of this variation and is given by the equation

$$\Delta q_{2\ \text{spectral}} = q_2' - q_2 \tag{9}$$

This error may be calculated if all terms in Eq. (7) and (8) are known.

Some difficulty may be encountered in evaluating the integrals in Eq. (7) and (8) to any degree of accuracy due to incompleteness of data on the parameters involved. Although data on $\alpha(\lambda)$ is available for some materials, work is continually underway to improve the measurements and extend them to other materials, since $\alpha(\lambda)$ is the backbone of any thermal analysis. The spectral energy distribution of the Sun, $I_s(\lambda)$, is normally taken to be that given by Johnson (Ref. 1). Data on the spectral energy distribution of most sources considered for use in solar simulators, $I_{ss}(\lambda)$, is rather difficult to obtain, since manufacturers seem rather reluctant to publish this data to the necessary accuracy. Even with data on $I_{ss}(\lambda)$, one is faced with the difficulty of trying to evaluate variations in $I_{ss}(\lambda)$ and $\alpha_n(\lambda)$ and $\tau_n(\lambda)$ of the optical elements in the system with operating time. At the present time, spectral data on these variations is virtually non-existent.

The problem of spectral energy absorption errors is further compounded by the diversity of characteristics possessed by the various materials normally used in temperature control. Four widely used surface treatments are commercially polished gold plating, commercially polished aluminum, white paints, and black paint. The first three are far from being grey bodies, having significantly different spectral absorptances for ultraviolet, visible, and infrared wavelengths. Gold has a high absorptance in the ultraviolet and visible regions, while its infrared absorptance is very low. Aluminum has its highest absorptance in the ultraviolet and its lowest absorptance in the infrared. White paints have higher absorptances in the ultraviolet and infrared than in the visible. Obviously, a close approximation to the solar spectrum is needed if the absorptance errors of all of these surfaces are to be small.

To demonstrate the effect of spectral errors on various materials, a computer program was written to evaluate the integrals in Eq. (7) and (8). Some very rough values of $\Delta q_{2\ \text{spectral}}/q_2$ obtained from the computer results are given in Table 4. The values presented in Table 4 are errors relative to the respective solar energy absorbed. Since these errors are a fraction of the solar energy absorbed, they will affect the temperature of nodes with low internal power dissipation more severely than those with high internal power dissipation. Note that in Table 4 only the 50% Hg-Xe-50% Xe system has less than a relative 10% error for all

five spacecraft surfaces. This system seems to have good possibilities. However, the calculations in this memorandum have been performed with the assumption of a carbon arc solar source. It should be pointed out that the values in Table 4 are approximate and do not take into account variations in fireball size and position with respect to optical elements in the system. Much work remains to be done on improvement of solar spectrum simulation both from a theoretical and a practical standpoint.

Table 4. Calculated absorptance error relative to solar absorptance, %

	1	2	3	4	5
Gold (polished)	+ 8.5	+ 30.9	+ 31	- 4.5	- 31.8
Aluminum (polished)	- 2.1	+ 8.5	+ 7.6	+ 0.3	- 1.4
ZW-60 white	+ 10	+ 8.8	- 12.4	+ 4.5	- 16.6
Aluminum paint	+ 2	+ 3.5	- 4	1.0	+ 1.7
Black paint	0	0	0	0	0

Column 1 – Carbon arc with one aluminum reflection and transmission through 2.4 in. of quartz.

Column 2 – Westinghouse Hg-Xe (bare).

Column 3 – Westinghouse Hg-Xe with one aluminum reflection and transmission through 1.6 in. of quartz.

Column 4 – 50% Westinghouse Hg-Xe, 50% Xe (bare).

Column 5 – Hannovia Xe (bare).

The error due to decollimation of the solar simulation source ($\Delta q_{2\ \mathrm{decollimation}}$) is a result of energy flux density variations in the test volume, blurring of shadows, and illumination of surfaces parallel to the Sun – probe line (sidelighting). Ideally, the decollimation angle of the solar simulation source should be that of the Sun (32 min of arc). However, this is obviously impractical at the present time, and the effects of larger decollimation angles will have to be accounted for. The sidelighting effect will be discussed under q_6 below.

Energy flux density variations in the test volume are the result of decollimation of the solar source and misalignment of the simulator optical system. Uniformity of flux density may be defined as the percent deviation of flux density from nominal over a given area. It is presently felt that a variation of ±5% in the longitudinal and radial directions of the test volume, measured with a detector area of 4 in.^{2} is an acceptable error. These figures, if attainable, should make it possible to neglect the secondary effects of the warped

spacecraft temperature field discussed below under q_4 and q_5. However, this variation would probably still not furnish sufficient uniformity to permit the use of Sun sensors during a spacecraft systems test.

Two examples of shadow blurring are given in Figs. 1 and 2. Figure 1 illustrates the shadow cast by a plane horizontal edge with a "Sun image" type of source. Obviously, the width of the blurred region is ($2h$ tan θ). Two difficulties resulting from this effect are apparent: (1) energy impinges on region AB, which would normally be completely shaded, and (2) region BC suffers from a reduced energy flux density. This could result in a fairly large error in absorbed energy for an object in the blurred region whose width is less than distance AC. This error would be reduced to zero if the shadow were to fall symmetrically on the object below. However, it may not always be possible to achieve such a configuration. In the *Ranger* Block II series, shading objects were commonly 3 to 4 ft above areas of critical thermal control. Thus, a 6-deg decollimation half-angle with a uniform source would result in a blurred region about 10 in. wide.

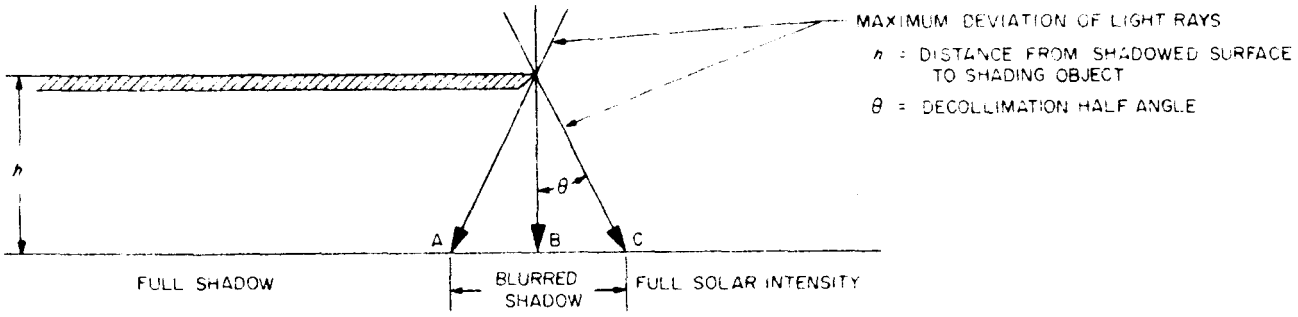

Fig. 1. Shadow formed by plane edge perpendicular to mean light ray in "Sun image" solar simulator

Another type of shadow, that cast by a flat plate parallel to the mean light ray, is shown in Fig. 2a. The width of the blurred region in this case will be h_1 tan θ + h_2 tan θ or (h_1 + h_2) tan θ. Region DE of the blurred area will be deficient in energy when compared to the case above. Some of the energy that would have impinged on DE will strike GH and be partially reflected to region EF of the blurred area. Depending on the surface treatment of GH, it may be possible to solve for the flux density distribution through the region EF. This would at least enable a ballpark calculation for an object in this region. A calculation was carried out on the effect of this type of shadow blurring on the *Ranger* Block III equipment mounting plates. The configuration used is shown in Fig. 2b. It was found that, neglecting energy reflected from surface GH, the solar input to the plate was approximately 12% less than in space with a solar simulator decollimation half-angle of 5.3 deg. For the purpose of the analysis in this memorandum, it may be assumed that the error due to shadow blurring will be of the order of 15% of the direct solar absorption for structural elements or scientific packages.

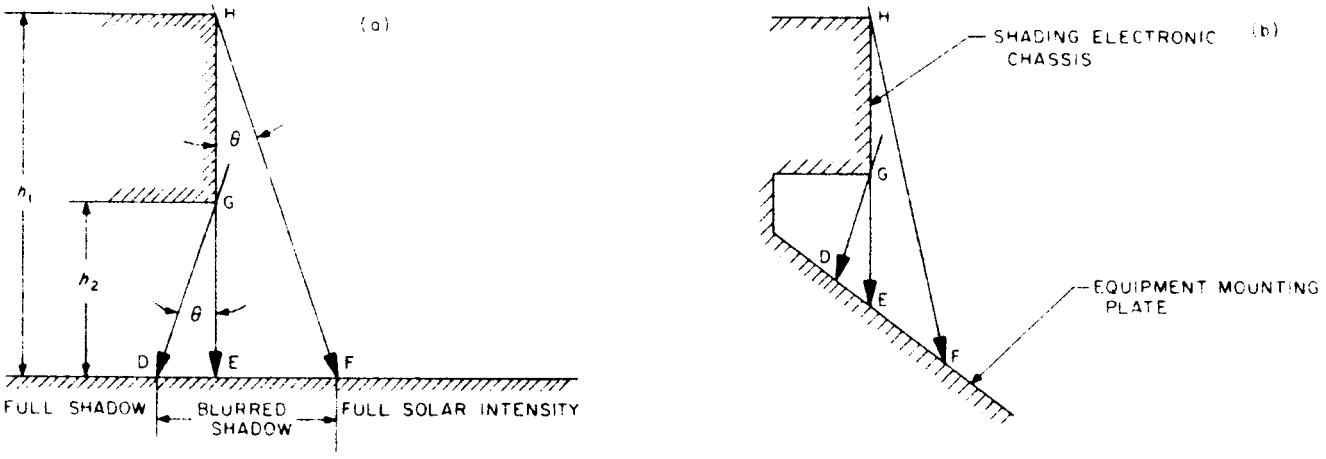

Fig. 2. Shadow formed by plane surface parallel to mean light ray in "Sun image" solar simulator

C. Absorption of Indirect Solar Energy, q_3

Indirectly incident solar energy may be defined as that solar energy striking a spacecraft surface which has previously undergone one or more reflections from other spacecraft surfaces. The nature of this reflected energy is complicated by two effects. The first effect is the change in spectral energy distribution of the incident energy upon reflection from a surface. Owing to the spectral reflectance characteristics of surfaces, this energy distribution will change on each reflection, affecting the energy absorbed on each reflection. The second effect is that of the increase in decollimation of the incident energy upon each reflection from a surface, the amount of increase depending on the characteristics of the surface. This is due to the fact that real surfaces are neither 100% specular nor 100% diffuse but, in fact, are somewhere between these limits.

The only analytical technique available to treat this phenomenon for spacecraft surfaces is the ray tracing technique. However, because of the complexity of reflected radiation, ray tracing is impractical even for the simple case of perfect light collimation. Obviously, the more complex cases where the incident energy is not perfectly collimated are definitely less likely to yield to ray tracing techniques. Therefore, the error due to absorption of indirect solar energy must be considered as the entire heat input from this effect until better techniques can be developed or sufficient flight data is received. Calculated estimates of this heat input for electronic assemblies, a typical science package, and a typical structural element are 1.5, 2.9, and 1.5 watts, respectively. It should be noted that these figures do not represent a worst case situation and, therefore, the heat input could be considerably greater. It is estimated from *Ranger* 3 flight data that 32% of

the solar energy absorbed by the gamma ray spectrometer was reflected from other spacecraft surfaces.

D. Intercepted Emission from Other Spacecraft Parts, q_4

If the spacecraft flight temperature field can be perfectly simulated in a test, then the error connected with this energy input to a node will be identically zero. However, this temperature field will probably not be perfectly simulated due to the combination of possible (and probable) errors discussed in this memorandum. The error connected with this term will tend to even out temperature variations in the spacecraft. Analytically, the value of this term can only be grossly estimated since the surfaces involved in this mode of heat transfer generally are not diffuse surfaces.

E. Spacecraft Interconduction, q_5

Except for the mechanism of heat transfer, the sources of error and the effect on the temperature field connected with this term are identical to those discussed for q_4 above. The errors associated with those two terms are the "secondary effect" of the axial and radial variations in solar simulation energy flux density and are the reason why the temperature effect of these variations on a spacecraft cannot be eliminated by energy flux mapping of the spacecraft surfaces.

F. Energy Absorbed by Surfaces Parallel to the Sun-Probe Line, q_6

Decollimation of the solar simulation source will result in an energy flux through planes parallel to the mean light ray (sidelighting). This energy flux is highly undesirable since these planes are primarily emitting surfaces on a Sun-oriented spacecraft. Table 5 lists the vertical surface areas typical of three *Ranger* objects and the heat input associated with these surfaces for three decollimation half-angles. These values were calculated from a set of curves by H. N. Riise (Ref. 2).

Table 5. Sidelighting energy absorbed by surfaces parallel to Sun – probe line for three values of solar simulator decollimation half-angle

Object	Area, ft^2	Heat Input, w		
		2 deg	4 deg	6 deg
Electronic assembly	2	0.44	0.91	1.35
Science box	1.5	0.35	0.67	1.00
Leg	1.4	0.32	0.62	0.94

G. Energy Reflected by the Spacecraft Back to the Solar Simulator and Rereflected to the Spacecraft, q_7

In space, solar energy reflected from surfaces approximately perpendicular to the Sun's rays will not normally impinge again on spacecraft surfaces. However, in some types of solar simulation systems, this reflected energy may be returned to the spacecraft by certain elements of the solar simulator. The large parabolic mirror of a cassegrain system would return this energy. A ray tracing analysis was performed on an IBM 7090 computer to determine the amount of this energy which returns to the spacecraft for the on-axis cassegrain system in the 25-ft Space Simulator. The "spacecraft" was taken to be a polished flat circular disc. The results of this program are presented in Table 6 for three levels—corresponding to the top, middle, and bottom of the working volume as defined by the original contract specification. As can be seen, a considerable amount of this energy would be returned to the spacecraft. A simple calculation shows that the average energy flux due to the first reflection pair on a 3-ft-radius polished aluminum disc 18 ft from the floor of the test chamber would be 53% of the originally incident energy! In general, these secondary rays return to the spacecraft at considerably greater incidence angles than the primary flux, thus causing errors due to multiple reflection absorption. The geometry of the system precludes their use as a bolstering factor for the main energy stream.

Table 6. Percent of reflected solar energy returned to spacecraft* by solar simulator optics in the original cassegrain design of the JPL 25-ft Space Simulator

Spacecraft diameter, ft	Distance from floor, ft	Radial Position of Reflecting Element, ft						
		0	1	2	3	4	5	6
6	10	80.6	57.1	29.9	8.3			
	14	81.5	75.7	70.4	29.2			
	18	73.6	67.8	67.8	56.7			
8	10	81.0	80.1	47.4	16.8	16.7		
	14	82.5	76.6	71.1	38.5	27.9		
	18	78.5	72.4	68.9	74.2	67.6		
10	10	81.3	80.4	76.7	24.6	30.2	40.1	
	14	83.7	78.6	71.7	39.0	77.1	21.6	
	18	84.5	76.2	70.0	74.2	78.2	85.6	
12	10	81.8	80.5	77.0	40.3	45.4	18.7	4.4
	14	85.1	79.9	73.6	39.2	77.1	76.0	12.2
	18	91.3	84.8	73.8	74.3	78.2	76.3	79.7

*Spacecraft assumed to be polished flat circular disc of diameter shown in first column.

H. Energy Emitted by the Spacecraft and Returned to the Spacecraft by the Solar Simulator, q_8

The presence of the large parabolic mirror in a cassegrain system will be felt by the spacecraft in the infrared regime as well as that of the solar simulation spectrum. As the nature of the emission from spacecraft surfaces is probably closer to diffuse than specular, a lower percentage of this energy will strike the mirror and correspondingly less will be returned to the spacecraft. Ray tracing has shown that approximately 10 to 15% of the energy emitted by an object at the top of the test volume would be returned. This effect becomes appreciable when the upper spacecraft surfaces are black, since the reflected solar energy discussed above is decreased immensely because of the high absorptance of the black surface. These two effects (q_7 and q_8) decrease to zero for an "off-axis" cassegrain system if the test volume does not intrude into the cone whose base is defined as the plane of the mirror edge and whose height is defined as twice the focal length of the mirror as shown in Fig. 3.

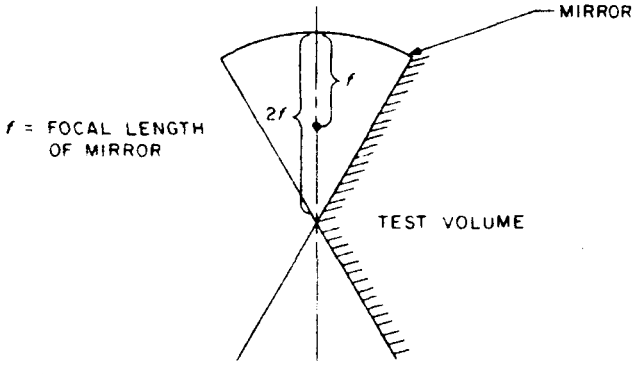

Fig. 3. Location of test volume for elimination of q_7 and q_8 errors

I. Energy Emitted by Various Optical Elements of the Solar Simulation System, q_9

The presence of various optical elements within the chamber will be felt by the spacecraft unless liquid nitrogen shrouds are provided to shield them. Mirrors will have a very small effect on a spacecraft because of their high reflectance and low emittance. An uncoated mirror at room temperature will emit 10 times more energy than a black shroud at −320°F but only 1/20th the energy of a black shroud at room temperature. In order for an uncoated mirror to emit the same amount of energy per unit area as a black shroud at −320°F, the mirror temperature must be approximately −164°F.

Transparent optical elements, however, have high emittances and could emit an appreciable amount of energy if not shielded or coated and operated at liquid nitrogen temperatures. Clearly, shielding may not be possible on systems which beam energy directly on the spacecraft, since shields would block the shorter

solar simulation wavelengths as well as the unwanted infrared. If at all possible, optical elements in the chamber should at least be operated at low temperatures in order to minimize these effects.

V. CONCLUSIONS

Specular multireflection between the spacecraft and large mirror of a cassegrain solar simulator is intolerable from a systems thermal testing standpoint. "Off center" cassegrain systems like the system presently in use in the JPL 25-ft Space Simulator not only remove the specular multireflection error, but also remove the infrared reflection error by eliminating the image of the spacecraft in the large mirror as seen from the spacecraft.

One system not mentioned above is the "bore-sighted" solar simulator. It may be shown by relatively simple trigonometric relations that boresighted systems of reasonable size have much higher errors resulting from sidelighting (Δq_b) than do "Sun image systems". In addition, the axial energy flux density variation is much larger and shadow malformation far more complex than in a Sun image system. These characteristics make boresighted systems look quite unattractive for thermal systems testing.

Of the errors associated with absorption of solar simulation energy, the error associated with spectral mismatch appears to be the largest. Work should definitely be continued toward the development of a permanent arc or combinations of arcs in various gases which closely approach the Johnson solar spectrum curve. An essential characteristic of any arc source is constancy of spectrum over periods of extended operation or numerous start-ups and shut-downs. A reliable scheme for monitoring the solar simulator spectral distribution during thermal systems tests should also be developed.

Improvement of the degree of decollimation of the solar source will reduce the errors associated with absorption of direct and reflected solar energy, shadow blurring, side lighting, and variation of uniformity of incident solar energy. In some rare cases, it may be possible to circumvent these errors by designing the spacecraft with solar simulator testing problems in mind. However, this generally will not be possible. Since analytical techniques cannot be used to determine all of the errors resulting from decollimation, it seems necessary to approximate the solar collimation angle (32 min) as accurately as is possible.

The information contained in the previous tables and discussion may be summarized in Tables 7, 8, and 9. Following is a summary of subscripts used in Tables 7, 8, and 9:

1 = electrical power dissipation

2 = direct solar energy absorbed

3 = reflected solar energy absorbed

4 = infrared energy absorbed from other spacecraft nodes

5 = conduction input from other spacecraft nodes

6 = energy absorbed due to sidelighting

7 = solar energy absorbed after reflection by spacecraft to optics and return

8 = energy emitted by spacecraft, returned to spacecraft by optics, and reabsorbed

9 = energy emitted by optics and absorbed by spacecraft

Table 7. Summation of heat inputs (in watts) based on space conditions

	q_1	q_2	q_3	q_4	q_5	Σq_n
Electronic assembly	17.6	9.7	1.5	0.6	1.5	30.9
Science package	0.6	13.2	2.9	0.6	0.6	17.9
Structural element (leg)	0.0	2.9	1.5	0.6	1.5	6.5

Table 8. Breakdown of Δq_2

	$\Delta q_{2\ \text{spectral}}$	$\Delta q_{2\ \text{decollimation}}$			Total, %	Δq_2, w
	Spectral mismatch, %	Vertical nonuniformity, %	Axial nonuniformity, %	Shadow malformation, %		
Electronic assembly	8.5 (gold)	5	5	0	18.5	1.8
Science package	8.5 (gold)	5	5	15	33.5	4.4
Structural element	8.5 (gold)	5	5	15	33.5	0.97

Table 9. Total Δq_n (in watts) and summation of Equation (6)

	Δq_1	Δq_2	Δq_3	$\Delta q_{4\ \&\ 5}$	Δq_6	$\Delta q_{7,\ 8,\ 9}$	$\Sigma \Delta q_n$	$\frac{\Sigma \Delta q_n}{\Sigma q_n}$
Electronic assembly	0.0	1.8	1.5	0.0	1.3	Designed out of chamber	4.6	0.14
Science package	0.0	4.4	2.9	0.0	1.0		8.3	0.44
Structural element	0.0	0.97	1.5	0.0	1.0		3.4	0.53

A comparison of the values in the last column of Table 9 with the summation of Eq. (5) indicates that a thermal test with solar simulation under the conditions stated here would provide meaningful data for major electronic assemblies. The data from smaller elements of the spacecraft such as structural elements and science packages would probably be less significant. The use of special paint patterns or nonflight modifications (heaters to make up for lack of solar energy or shields to guard against too much solar input) would aid science packages or structural elements in operating near flight cruise temperatures. However, careful test data analysis using well defined system operating parameters is necessary in order to meaningfully interpret the test results.

APPENDIX A

Revision of Tables Reflecting *Ranger* Block III Design

The tables in the main body of this memorandum were based principally on the thermal design characteristics of the *Ranger* Block II spacecraft. These tables have been revised (Tables A1 – A9) to reflect the thermal design characteristics of the *Ranger* Block III spacecraft. Where applicable, new data on solar absorptances, etc., have been included.

The average unknown in emittance for *Ranger* Block III electronic chassis is 3%. Tolerance imposed on flight cruise temperatures is ± 40°F about a nominal 85°F. Recalculated analytical value of $\Sigma \Lambda q_n / \Sigma q_n$ (Eq. 5):

$$\frac{\Sigma \Lambda q_n}{\Sigma q_n} = \pm 0.03 + 4\left(\frac{40}{545}\right) = \pm 0.26 \qquad \text{(A5)}$$

Table A1. Absolute emittance and relative uncertainty of typical spacecraft surfaces

Material	Absolute emittance	Relative uncertainty, %
Black paint	0.90 ± 0.02	2
White paint (PV 100)	0.85 ± 0.02	2
White paint (JW 40)	0.78 ± 0.02	3
Aluminum paint	0.30 ± 0.03	10
Polished aluminum (commercial polish)	0.045 ± 0.005	11
Gold plate	0.035 ± 0.005	14

Table A2. Average power dissipations for three spacecraft elements, q_1

Object	Power dissipation, w
Major electronic assembly	14.2 to 31.6
Science package	0.1 to 1.0
Structure	0

Table A3. Solar energy absorbed by three spacecraft elements, q_2

Object	Energy absorbed, w
Major electronic assembly (Average of 5 *Ranger* Block III chassis)	27.7
Science assembly	5.0 to 20
Structure (*Ranger* leg)	2.3

Table A4. Deviation of absorptance in mercury-xenon spectrum from solar absorptance

See Table B1 (Appendix B)

Table A5. Sidelighting energy absorbed by surfaces parallel to Sun-probe line for three values of solar simulator decollimation half-angle, watts

Object	Area, ft^2	2 deg	4 deg	6 deg
Electronic assembly	2.0	0.62	1.25	1.88
Science box	1.5	0.36	0.72	1.08
Leg	1.4	0.27	0.54	0.81

Note: The values of energy absorbed in this table differ from those in Table 5 on page 13 owing to the use of absorptance values obtained in the JPL 25-ft Space Simulator (Table B1) and the surface coatings used in the *Ranger* Block III thermal design.

Table A6. Percent of reflected solar energy returned to spacecraft by solar simulator optics in the original cassegrain design of the JPL 25-ft Space Simulator

Same as Table 6, page 14.

Table A7. Summation of heat inputs (in watts) based on space conditions

	q_1	q_2	q_3	q_4	q_5	Σq_n
Electronic assembly	27.0	27.7	2.0	1.0	2.0	60.0
Science package	0.6	13.2	2.9	0.6	0.6	17.9
Structure	0.0	2.9	1.5	0.6	1.5	6.5

Table A8. Breakdown of Δq_2

	Δq_2 spectral	Δq_2 decollimation				
	Spectral mismatch, %	Vertical nonuniformity, %	Axial nonuniformity, %	Shadow malformation, %	Total, %	Δq_2, watts
Electronic assembly	0 (black)	5	5	0	10	2.8
Science package	19 (gold)	5	5	15	44	5.8
Structure	16 (aluminum)	5	5	15	41	1.2

Table A9. Total Δq (in watts) and summation of Equation (6)

	Δq_1	Δq_2	Δq_3	$\Delta q_{4\ \&\ 5}$	Δq_6	$\Delta q_{7,\ 8,\ 9}$	Δq_n	$\frac{\Sigma \Delta q_n}{\Sigma q_n}$
Electronic assembly	0	2.8	2.0	0	0.6	Designed out of chamber	5.4	0.09
Science package	0	5.8	2.9	0	0.4		9.1	0.51
Structure	0	1.2	1.5	0	0.3		3.0	0.46

APPENDIX B
Some Comments on Recent Thermal Tests in the JPL 25-ft Space Simulator

Since the original work was done on this report, four thermal tests have been carried out in the JPL 25-ft Space Simulator by the *Ranger* thermal groups of JPL and RCA. The objects tested were a thermal model of the RCA television subsystem, a complete thermal model of the *Ranger* Block III spacecraft (tested twice), and the *Ranger* Block III proof test model. Some of the effects discussed in the preceding pages were encountered during these tests and are discussed below.

Decollimation of the solar simulation source resulted in probably the most significant problem encountered during this series of tests. Two preliminary investigations into the effect of decollimation on the RCA subsystem were performed before the RCA Temperature Control Model (TCM) was suspended in the simulator. A special large-aperture camera was used to photograph the solar simulator light source to obtain an estimate of the degree of decollimation of the source. In addition, a test fixture simulating the fin configuration of the TCM was examined under the solar simulation light beam. With the data obtained from these investigations, together with incident energy flux mapping data obtained from the TCM in the light beam, it was hoped to determine the amount of energy reflected from the conical skin of the RCA TCM onto the annular fins. When the TCM was illuminated by the solar simulator, approximately 40% of the polished aluminum skin was partially illuminated by the solar source. In space, the fins would completely shade the skin. The thermal vacuum test of the RCA TCM resulted in an average equilibrium temperature approximately 40°F higher than that predicted for flight (63°F). Even with the data obtained from the two preliminary investigations and the energy flux mapping of the RCA TCM itself, 16% of the energy absorbed by the subsystem in the thermal vacuum test could not be accounted for.

After analysis of the RCA TCM test results, the following recommendations were made:

1. Eliminate directly incident decollimated light from striking the skin of the TCM.
2. Improve the instrumentation used for determination of energy flux density.

These recommendations were implemented for the first test of the complete *Ranger* Block III TCM (JPL bus with RCA subsystem attached). Fin extensions were added to the RCA subsystem solar absorbing fins, increasing the effective width of these fins. These extensions were attached so as not to add to the energy absorbed by the fins themselves and were trimmed to a width which would shade the polished aluminum skin

of the subsystem from directly incident energy. A thermopile was used in this test to monitor solar simulation flux density, replacing the solar cell used in the first test of the RCA TCM. Although the average equilibrium temperature of the RCA subsystem under solar simulation in this test was considerably lower than the predicted flight temperature, 100% of the energy input to the subsystem could be accounted for. This was a significant improvement over the results of the first RCA TCM test. The lower-than-flight temperature in this test resulted from partial blockage of directly incident solar energy on the TCM fins and, in some locations, partial shadowing of the fin by the ring on the fin above.

When the solar simulator lights were initially turned on for the complete TCM, the white surfaces on the fronts of the electronic chassis were illuminated due to decollimation of the solar simulation source. Based on the difficulties encountered with the RCA TCM in the first test, shading strips or "eyebrows" were added to the tops of the cases to eliminate illumination of the vertical case surfaces. The energy flux on the fronts of the cases was reduced considerably by these "eyebrows."

Values of absorptance in the mercury-xenon spectrum of the 25-ft Space Simulator were experimentally evaluated through the use of a "button box" developed at JPL (Ref. 3). The mercury-xenon absorptances were used in evaluating the test data obtained in the TCM tests and PTM test. The absorptance values obtained, together with their respective solar absorptances (calculated from the Johnson curve), are listed in Table B1. The mercury-xenon absorptances are thought to be accurate to ± 10%.

Table B1. Comparison of measured Hg-Xe absorptances in JPL 25-ft Space Simulator with calculated solar absorptances for several spacecraft surface treatments

Surface	Solar α	Hg-Xe α	Percent Error
Polished gold	0.22	0.263	+ 19.5
Polished aluminum	0.185	0.214	+ 15.7
Cat-a-lac black paint	0.96	0.962	- 0.2
JW-40 white paint	0.225	0.387	+ 72.0
RCA No. 1 (white with 0.7% black)	0.37	0.43	+ 16.2
RCA No. 2 (white with 3.2% black)	0.55	0.58	+ 5.5
RCA No. 3 (white with 12.9% black)	0.76	0.82	+ 7.9
RCA No. 4 (PV-100 white)	0.22	0.31	+ 41.0

Energy flux mapping of the spacecraft surfaces was performed before each thermal test. The purpose of the mapping was to furnish data on directly incident and reflected solar energy for the various spacecraft surfaces. As stated previously, this mapping did not eliminate the errors due to a warped spacecraft temperature field. However, it did facilitate the calculation of solar energy absorbed on various portions of the spacecraft in the analysis of test data. Unfortunately, the accuracy of these calculations is limited by the accuracy of the mapping data, which is estimated to be ± 5 watts ft^2.

More detailed descriptions of these tests may be found in Refs. 4 – 7.

REFERENCES

1. Johnson, F. S., "The Solar Constant," *Journal of Meteorology*, Vol. II, No. 6, December 1954, pp. 431-439.

2. Personal communication from H. N. Riise, Jet Propulsion Laboratory.

3. Personal correspondence with D. W. Lewis, Jet Propulsion Laboratory.

4. Lerner, M., "*Ranger* Block III Temperature Control Report on Thermal Control Model Tests (Phase I) in 25-ft Space Simulator With Use of Solar Lights," JPL interoffice document, August 1, 1963.

5. Lerner, M., "*Ranger* Block III Temperature Control Report On Thermal Control Model Tests (Phase II) in 25-ft Space Simulator," JPL interoffice document, August 30, 1963.

6. Lerner, M., "*Ranger* Block III Temperature Control Report on Proof Test Model Tests," JPL interoffice document, November 11, 1963.

7. *Ranger TV Subsystem, Block III*, Thirteenth Bimonthly Progress Report, Radio Corporation of America, October 8, 1963.

Prepared Under Contract No. NAS 7-100
National Aeronautics & Space Administration

CONTENTS

TABLES

TABLES (Cont'd)

FIGURES

PREFACE

The original work on this report was done by L.B. Katter before he left JPL in December 1962. At that time, the *Ranger* Block II program was essentially completed. The temperature control design of the *Ranger* Block III spacecraft had not been completed. For this reason, most of the numerical values for power dissipation, surface properties, etc., used for calculations in the original draft of the report, reflected the thermal design of the *Ranger* Block II spacecraft. When work was resumed on the report, it was decided to leave the numerical calculations as they were and to supplement them with an appendix reflecting the *Ranger* Block III thermal design. The revised calculations are contained in Appendix A.

Since the completion of the *Ranger* Block II program, four thermal tests with solar simulation have been performed in the JPL 25-ft Space Simulator by the *Ranger* temperature control group. In Appendix B, some comments are made relative to problems encountered in performing these tests and analyzing the results.

Technical Memorandum No. 33-175

The Effect of Solar Simulator Operating Characteristics on Spacecraft Thermal Tests

L. B. Katter
M. E. Kahn

JET PROPULSION LABORATORY
CALIFORNIA INSTITUTE OF TECHNOLOGY
PASADENA, CALIFORNIA

July 15, 1964

ABSTRACT

19136

A study has been made to determine the effect of various solar simulator operating characteristics on spacecraft thermal tests. Characteristics considered are: (1) the effects of decollimation, (2) spectral mismatch, and (3) axial and radial variations of energy flux density. In addition, the effect of solar simulator optics in the chamber has been considered for certain special cases.

I. INTRODUCTION

At the present time, spacecraft thermal control design is based primarily on analysis. Practicality limits the number of pieces into which the spacecraft can be separated for analysis and the degree of detail with which these individual pieces of the spacecraft may be analyzed. The capability of handling more of this analysis by computer techniques is being developed. However, the uncertainties in solar absorptance, emittance, joint conductance, and internal power dissipation, coupled with the difficulty of calculating combined specular and diffuse heat transfer, limit the solutions to the prediction of a relatively wide span for steady-state flight temperatures and transient temperatures. A *valid* experimental verification of the analytically determined thermal design is highly desirable and could result in a reduction in the required operating temperature range for many of the spacecraft electronic components, thus increasing spacecraft reliability.

For any constant temperature portion of a spacecraft (node) radiating to space at steady state, the temperature of the node will be defined by the statement of energy conservation

$$\Sigma q_n = A \bar{\epsilon} \sigma T^4 \qquad (1)$$

where

Σq_n = net heat input to the node

A = the external radiating area of the node

$\bar{\epsilon}$ = the average emittance of the node

T = the absolute temperature of the node

σ = the Stephan-Boltzmann constant

Taking the logorithm and then the differential of Eq. (1) gives

$$\frac{\Delta \Sigma q_n}{\Sigma q_n} = \frac{\Delta A}{A} + \frac{\Delta \bar{\epsilon}}{\bar{\epsilon}} + 4\frac{\Delta T}{T} \tag{2}$$

Assuming that the external area is known (or can be measured) with negligible error ($\Delta A = 0$), Eq. (2) reduces to

$$\frac{\Delta \Sigma q_n}{\Sigma q_n} = \frac{\Delta \bar{\epsilon}}{\bar{\epsilon}} + 4\frac{\Delta T}{T} \tag{3}$$

The conservative assumption that the errors in the individual terms making up Eq. (3) should be added in a scalar manner rather than statistically yields

$$\frac{\Sigma \Delta q_n}{\Sigma q_n} = \frac{\Delta \bar{\epsilon}}{\bar{\epsilon}} + 4\frac{\Delta T}{T} \tag{4}$$

This form of the statement of energy conservation will be useful for the discussion to follow.

The information of primary interest in analysis and thermal testing of a spacecraft is the temperature distribution among the various spacecraft nodes. Equation (1) may be rearranged to show the dependence of temperature deviation from nominal flight temperature on variation of emittance and net heat input to a node.

$$\frac{\Delta T}{T} = \frac{1}{4}\left[\frac{\Sigma \Delta q_n}{\Sigma q_n} - \frac{\Delta \bar{\epsilon}}{\bar{\epsilon}}\right] \tag{1'}$$

It can be seen that a decrease in emittance has the same effect on temperature as an increase in net heat input. Thus, the worst temperature deviation will occur when $\Sigma \Delta q_n$, Σq_n, and $\Delta \bar{\epsilon}$ are of opposite sign.

In appraising the value of solar simulator testing in relation to analysis, it is more convenient to examine the variations of heat input to a node rather than variations in temperature. An estimate of the error in the calculated heat input to a node may be obtained by evaluation of the terms on the right side of Eq. (1). This error may be compared with the estimated error in heat input during solar simulator testing.

II. HEAT INPUT ERROR IN ANALYSIS

The design operating temperature for most spacecraft electronics is 85 F, with an allowable temperature range of −13 F. In thermal design calculations, an attempt was made in the past to design to a temperature as close as possible to the design operating temperature or to the mean of the upper and lower temperature limits for a given mode. As previously mentioned, these calculations result in a relatively wide spread for steady-state flight temperatures and maneuver transient temperatures. Under worst case conditions, ΔT for the mode could be as large as 13 F about a nominal 65 F during steady-state (cruise) operation.

Table 1 lists the emittances of six surface treatments used on the *Ranger* spacecraft. The uncertainties shown are still near the resolving power of the instruments used to measure the emittances of the surfaces.

Table 1. Absolute emittance and relative uncertainty of typical spacecraft surfaces

Material	Absolute emittance	Relative uncertainty, %
Black paint	0.90 ± 0.02	2
White paint (PV 100)	0.85 ± 0.02	2
White paint (JW 40)	0.78 ± 0.02	3
Aluminum paint	0.30 ± 0.03	10
Polished aluminum (commercial polish)	0.045 ± 0.005	11
Gold plate	0.035 ± 0.005	14

The desired average emittance of the *Ranger* Block II spacecraft electronic assemblies fell between 0.8 and 0.9. These emittances were achieved by mosaics of white paint applied to gold plate or commercially polished aluminum. For this range of emittances, the unknown would be 11% to 12% respectively, with 6% corresponding to the midrange.

The variations of emittance and temperature associated with analytical design were discussed in the preceding paragraphs. These values may be used in Eq. (4) with the sign relationships discussed to obtain a worst-case error for $\Sigma \Delta x_i \Sigma \varepsilon_i$ under the condition of worst temperature deviation:

$$\frac{\Sigma \Delta q_n}{\Sigma q_n} = \mp 0.06 + 4\left(\pm \frac{43}{545}\right) = \pm 0.26 \quad (5)$$

Thus, if solar simulator testing is to provide a significant improvement over analysis, the total heat input to the node in question must be within ±26% of its flight value. The possible sources of errors in heat input during solar simulator testing will be discussed below.

III. SOURCES OF HEAT INPUT

In space, the sources of heat input to a spacecraft node are the following:

1. Electrical power dissipation.
2. Absorption of directly incident solar energy.
3. Absorption of indirectly incident (reflected) solar energy.
4. Intercepted infrared emission from other spacecraft parts.
5. Net conduction from other spacecraft parts.

During a vacuum thermal test with solar simulation, each of these five inputs will be simulated with some error. In addition to these inputs, some additional "un-space-like" inputs will occur during testing. These un-space-like inputs can be broken into the following classes:

6. Energy absorbed on surfaces parallel to the Sun – probe line due to decollimation of the solar simulator.
7. Energy reflected by the spacecraft back to the solar simulator and rereflected again to the spacecraft.
8. Energy emitted by the spacecraft and returned to the spacecraft in a manner similar to that of the preceding input.
9. Energy emitted by the various optical elements of the solar simulation system.
10. Energy reflected and emitted by the cold (−320°F) black wall shroud.

The errors associated with the above inputs to a subassembly may be compensating, accumulative, or negligible, depending strongly on the spacecraft configuration and on the geometry of the subassembly. A summation of the differences between the values of terms 1–5 in a solar simulator test and their respective counterparts in space and of the values of terms 6–9 will give a conservative value of $\Sigma \Delta q_s$. Input 10 will not be included in the summation since it is mainly a function of chamber geometry (which is not considered in this memorandum) and is relatively insensitive to the quality of solar simulation. The preceding summation may be divided by a summation of space inputs 1–5 to arrive at a value of $\Sigma \Delta q_s \geq q_s$. Thus,

$$\begin{aligned} \Sigma \Delta q_s &= \Delta q_1 + \Delta q_2 + \Delta q_3 + \Delta q_4 + \Delta q_5 + \Delta q_6 + \Delta q_7 + \Delta q_8 + \Delta q_9 \\ \Sigma q_s &\qquad\qquad q_1 + q_2 + q_3 + q_4 + q_5 \end{aligned} \tag{6}$$

This summation may be compared with the value determined above in Eq. (5).

IV. TERM-BY-TERM DISCUSSION OF HEAT INPUTS

A. Electrical Power Dissipation, q_1

Sources of differences between electrical power dissipation in space and in a test chamber are non-flight hardware, ground-type power systems, and power through instrumentation cabling during these tests. A continuing effort to minimize these sources of error seems to have reduced them to a negligible magnitude. As for measurement of q_1, itself, we are not so well off. Measuring techniques and statistical variations of sub-components preclude an exact measurement of q_1. At this time most power measurements are thought to be accurate to ±5%. A typical set of power dissipations for the *Ranger* Block II spacecrafts is given in Table 2.

Table 2. Average power dissipation for three spacecraft elements, q_1

Object	Power dissipation, w
Major electronic assembly	4.4 to 26.4
Scientific package	0.03 to 0.88
Structure	0

B. Direct Solar Absorption, q_2

In space, 130 watts of solar energy per square foot of normal area is nominally incident at the Earth's mean distance from the Sun. The fraction of this energy (α) absorbed by a surface in space depends strongly on the surface properties and configuration with respect to the Sun. Table 3 shows the solar energy typically absorbed (q_2) by various *Ranger* objects during flight. During thermal vacuum tests with solar simulation, errors in "solar" energy absorbed will arise because of imperfect spectral match and imperfect collimation (decollimation) of the solar simulator. For purposes of analysis, it becomes convenient to separate these errors so that $\Delta q_2 = \Delta q_{2\ \text{spectral}} + \Delta q_{2\ \text{decollimation}}$. A discussion of each of these errors will follow.

The term $\Delta q_{2\ \text{spectral}}$ may be interpreted as the difference between the energy absorbed per unit normal area in space and that absorbed in a space simulator. The energy absorbed by a surface in space per unit normal area is given by the integral

$$q_2 = \int_0^\infty \alpha(\lambda) I_s(\lambda)\, d\lambda \qquad (7)$$

Table 3. Solar energy absorbed by three spacecraft elements, q_2

Object	Solar energy absorbed, w
Major electronic assembly (average for 6 chassis, *Ranger* Block II)	9.7
Science assembly (*Ranger* Block I)	8.8 to 20.5
Structure (*Ranger* leg)	2.9

where

λ = wavelength

$\alpha(\lambda)$ absorptance of material at wavelength λ

$I_\lambda(\lambda)$ flux density of solar radiant energy per unit area and unit wavelength at wavelength λ

In a solar simulator the energy absorbed per unit normal area is given by the integral

$$q_2' = \int_0^\infty \alpha(\lambda)\, I_{s\lambda}(\lambda)\, \rho_1(\lambda)\, \rho_2(\lambda) \cdots \rho_n(\lambda)\, \tau_1(\lambda)\, \tau_2(\lambda) \cdots \tau_k(\lambda)\, d\lambda \qquad (8)$$

where

λ wavelength

$\alpha(\lambda)$ absorptance of material at wavelength λ

$I_{s\lambda}(\lambda)$ flux density of solar simulator light source radiant energy per unit area and unit wavelength at wavelength λ

$\rho_n(\lambda)$ reflectance of nth mirror element in optical system at wavelength λ

$\tau_k(\lambda)$ transmittance of nth window or lens in optical system at wavelength λ

Notice that in Eq. (7) the energy absorbed is the integral of the product of the spectral absorptance and the spectral energy distribution of the source or Sun. Equation (8) has the same form as Eq. (7), the bracketed quantity being the effective spectral distribution of the solar simulation source in the test volume after having been modified by reflections and transmissions in the solar simulator optics. Thus, for a given surface [$\alpha(\lambda)$ fixed] the energy absorbed in various energy spectrums may vary greatly, depending on the spectral

characteristics of the source. The error $\Delta q_{2\ \text{spectral}}$ is the result of this variation and is given by the equation

$$\Delta q_{2\ \text{spectral}} = q_2' - q_2 \tag{9}$$

This error may be calculated if all terms in Eq. (7) and (8) are known.

Some difficulty may be encountered in evaluating the integrals in Eq. (7) and (8) to any degree of accuracy due to incompleteness of data on the parameters involved. Although data on $\alpha(\lambda)$ is available for some materials, work is continually underway to improve the measurements and extend them to other materials, since $\alpha(\lambda)$ is the backbone of any thermal analysis. The spectral energy distribution of the Sun, $I_{s\lambda}$, is normally taken to be that given by Johnson (Ref. 1). Data on the spectral energy distribution of most sources considered for use in solar simulators, $I_{s\lambda}(\lambda)$, is rather difficult to obtain, since manufacturers seem rather reluctant to publish this data to the necessary accuracy. Even with data on $I_{s\lambda}(\lambda)$, one is faced with the difficulty of trying to evaluate variations in $I_{s\lambda}(\lambda)$ and $\rho_n(\lambda)$ and $\tau_n(\lambda)$ of the optical elements in the system with operating time. At the present time, spectral data on these variations is virtually non-existent.

The problem of spectral energy absorption errors is further compounded by the diversity of characteristics possessed by the various materials normally used in temperature control. Four widely used surface treatments are commercially polished gold plating, commercially polished aluminum, white paints, and black paint. The first three are far from being grey bodies, having significantly different spectral absorptances for ultraviolet, visible, and infrared wavelengths. Gold has a high absorptance in the ultraviolet and visible regions, while its infrared absorptance is very low. Aluminum has its highest absorptance in the ultraviolet and its lowest absorptance in the infrared. White paints have higher absorptances in the ultraviolet and infrared than in the visible. Obviously, a close approximation to the solar spectrum is needed if the absorptance errors of all of these surfaces are to be small.

To demonstrate the effect of spectral errors on various materials, a computer program was written to evaluate the integrals in Eq. (7) and (8). Some very rough values of $\Delta q_{2\ \text{spectral}}/q_2$ obtained from the computer results are given in Table 4. The values presented in Table 4 are errors relative to the respective solar energy absorbed. Since these errors are a fraction of the solar energy absorbed, they will affect the temperature of nodes with low internal power dissipation more severely than those with high internal power dissipation. Note that in Table 4 only the 50% Hg-Xe-50% Xe system has less than a relative 10% error for all

five spacecraft surfaces. This system seems to have good possibilities. However, the calculations in this memorandum have been performed with the assumption of a carbon arc solar source. It should be pointed out that the values in Table 4 are approximate and do not take into account variations in fireball size and position with respect to optical elements in the system. Much work remains to be done on improvement of solar spectrum simulation both from a theoretical and a practical standpoint.

Table 4. Calculated absorptance error relative to solar absorptance, %

	1	2	3	4	5
Gold (polished)	+ 8.5	+ 30.9	+ 31	+ 4.5	31.8
Aluminum (polished)	- 2.1	+ 8.5	- 7.6	+ 0.3	1.4
ZW-60 white	- 10	- 8.8	- 12.4	+ 4.5	16.6
Aluminum paint	+ 2	+ 3.5	4	1.0	- 1.7
Black paint	0	0	0	0	0

Column 1 – Carbon arc with one aluminum reflection and transmission through 2.4 in. of quartz.

Column 2 – Westinghouse Hg-Xe (bare).

Column 3 – Westinghouse Hg-Xe with one aluminum reflection and transmission through 1.6 in. of quartz.

Column 4 – 50% Westinghouse Hg-Xe, 50% Xe (bare).

Column 5 – Hannovia Xe (bare).

The error due to decollimation of the solar simulation source ($\Delta q_{2\ \text{decollimation}}$) is a result of energy flux density variations in the test volume, blurring of shadows, and illumination of surfaces parallel to the Sun – probe line (sidelighting). Ideally, the decollimation angle of the solar simulation source should be that of the Sun (32 min of arc). However, this is obviously impractical at the present time, and the effects of larger decollimation angles will have to be accounted for. The sidelighting effect will be discussed under q_6 below.

Energy flux density variations in the test volume are the result of decollimation of the solar source and misalignment of the simulator optical system. Uniformity of flux density may be defined as the percent deviation of flux density from nominal over a given area. It is presently felt that a variation of ±5% in the longitudinal and radial directions of the test volume, measured with a detector area of 4 in.^{2} is an acceptable error. These figures, if attainable, should make it possible to neglect the secondary effects of the warped

spacecraft temperature field discussed below under q_4 and q_5. However, this variation would probably still not furnish sufficient uniformity to permit the use of Sun sensors during a spacecraft systems test.

Two examples of shadow blurring are given in Figs. 1 and 2. Figure 1 illustrates the shadow cast by a plane horizontal edge with a "Sun image" type of source. Obviously, the width of the blurred region is $(2h \tan \theta)$. Two difficulties resulting from this effect are apparent: (1) energy impinges on region AB, which would normally be completely shaded, and (2) region BC suffers from a reduced energy flux density. This could result in a fairly large error in absorbed energy for an object in the blurred region whose width is less than distance AC. This error would be reduced to zero if the shadow were to fall symmetrically on the object below. However, it may not always be possible to achieve such a configuration. In the *Ranger* Block II series, shading objects were commonly 3 to 4 ft above areas of critical thermal control. Thus, a 6-deg decollimation half-angle with a uniform source would result in a blurred region about 10 in. wide.

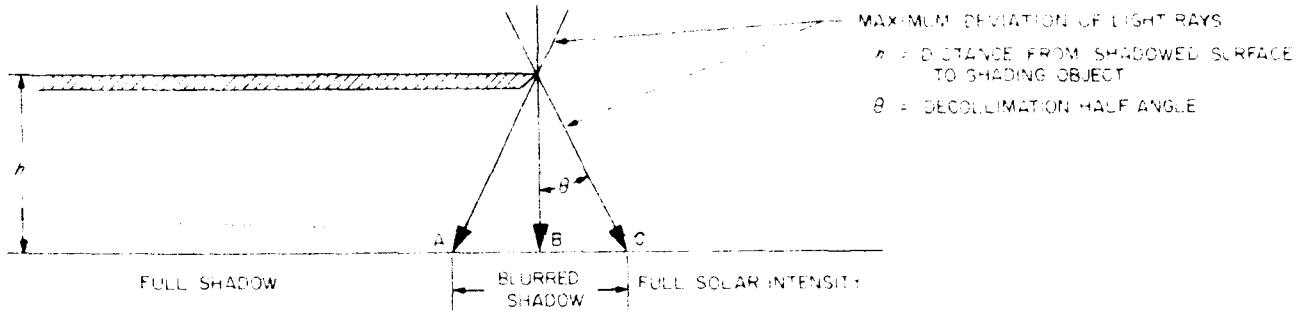

Fig. 1. Shadow formed by plane edge perpendicular to mean light ray in "Sun image" solar simulator

Another type of shadow, that cast by a flat plate parallel to the mean light ray, is shown in Fig. 2a. The width of the blurred region in this case will be $h_1 \tan \theta + h_2 \tan \theta$ or $(h_1 + h_2) \tan \theta$. Region DE of the blurred area will be deficient in energy when compared to the case above. Some of the energy that would have impinged on DE will strike GH and be partially reflected to region EF of the blurred area. Depending on the surface treatment of GH, it may be possible to solve for the flux density distribution through the region EF. This would at least enable a ballpark calculation for an object in this region. A calculation was carried out on the effect of this type of shadow blurring on the *Ranger* Block III equipment mounting plates. The configuration used is shown in Fig. 2b. It was found that, neglecting energy reflected from surface GH, the solar input to the plate was approximately 12% less than in space with a solar simulator decollimation half-angle of 5.3 deg. For the purpose of the analysis in this memorandum, it may be assumed that the error due to shadow blurring will be of the order of 15% of the direct solar absorption for structural elements or scientific packages.

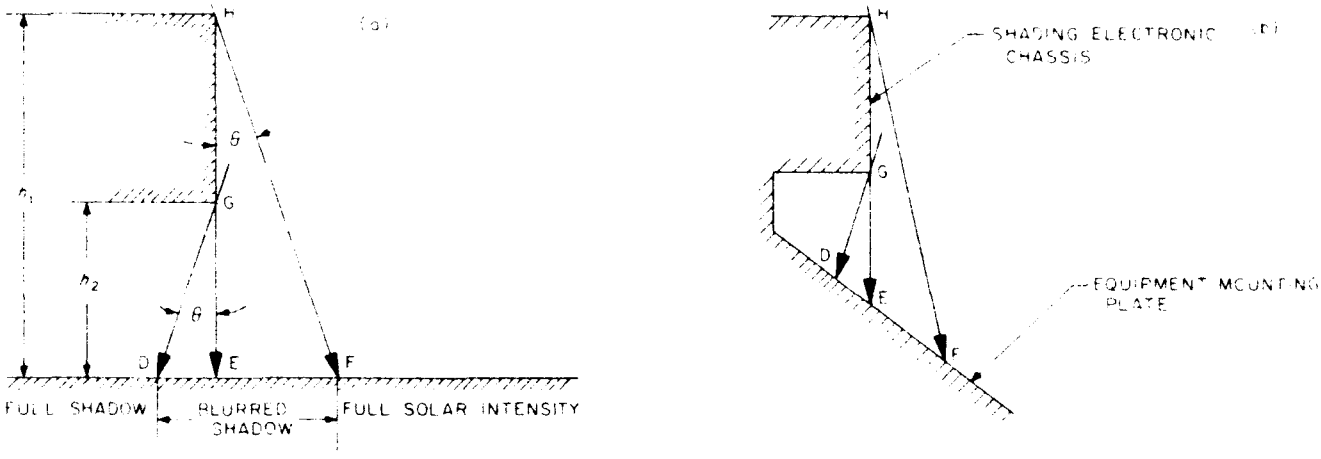

Fig. 2. Shadow formed by plane surface parallel to mean light ray in "Sun image" solar simulator

C. Absorption of Indirect Solar Energy, q_3

Indirectly incident solar energy may be defined as that solar energy striking a spacecraft surface which has previously undergone one or more reflections from other spacecraft surfaces. The nature of this reflected energy is complicated by two effects. The first effect is the change in spectral energy distribution of the incident energy upon reflection from a surface. Owing to the spectral reflectance characteristics of surfaces, this energy distribution will change on each reflection, affecting the energy absorbed on each reflection. The second effect is that of the increase in decollimation of the incident energy upon each reflection from a surface, the amount of increase depending on the characteristics of the surface. This is due to the fact that real surfaces are neither 100% specular nor 100% diffuse but, in fact, are somewhere between these limits.

The only analytical technique available to treat this phenomenon for spacecraft surfaces is the ray tracing technique. However, because of the complexity of reflected radiation, ray tracing is impractical even for the simple case of perfect light collimation. Obviously, the more complex cases where the incident energy is not perfectly collimated are definitely less likely to yield to ray tracing techniques. Therefore, the error due to absorption of indirect solar energy must be considered as the entire heat input from this effect until better techniques can be developed or sufficient flight data is received. Calculated estimates of this heat input for electronic assemblies, a typical science package, and a typical structural element are 1.5, 2.9, and 1.5 watts, respectively. It should be noted that these figures do not represent a worst case situation and, therefore, the heat input could be considerably greater. It is estimated from *Ranger* 3 flight data that 32% of

the solar energy absorbed by the gamma ray spectrometer was reflected from other spacecraft surfaces.

D. Intercepted Emission from Other Spacecraft Parts, q_4

If the spacecraft flight temperature field can be perfectly simulated in a test, then the error connected with this energy input to a node will be identically zero. However, this temperature field will probably not be perfectly simulated due to the combination of possible (and probable) errors discussed in this memorandum. The error connected with this term will tend to even out temperature variations in the spacecraft. Analytically, the value of this term can only be grossly estimated since the surfaces involved in this mode of heat transfer generally are not diffuse surfaces.

E. Spacecraft Interconduction, q_5

Except for the mechanism of heat transfer, the sources of error and the effect on the temperature field connected with this term are identical to those discussed for q_4 above. The errors associated with those two terms are the "secondary effect" of the axial and radial variations in solar simulation energy flux density and are the reason why the temperature effect of these variations on a spacecraft cannot be eliminated by energy flux mapping of the spacecraft surfaces.

F. Energy Absorbed by Surfaces Parallel to the Sun-Probe Line, q_6

Decollination of the solar simulation source will result in an energy flux through planes parallel to the mean light ray (sidelighting). This energy flux is highly undesirable since these planes are primarily emitting surfaces on a Sun-oriented spacecraft. Table 5 lists the vertical surface areas typical of three *Ranger* objects and the heat input associated with these surfaces for three decollimation half-angles. These values were calculated from a set of curves by H. N. Riise (Ref. 2).

Table 5. Sidelighting energy absorbed by surfaces parallel to Sun – probe line for three values of solar simulator decollimation half-angle

Object	Area, ft^2	Heat Input, w		
		2 deg	4 deg	6 deg
Electronic assembly	2	0.44	0.91	1.35
Science box	1.5	0.35	0.67	1.00
Leg	1.4	0.32	0.62	0.94

G. Energy Reflected by the Spacecraft Back to the Solar Simulator and Rereflected to the Spacecraft, q_7

In space, solar energy reflected from surfaces approximately perpendicular to the Sun's rays will not normally impinge again on spacecraft surfaces. However, in some types of solar simulation systems, this reflected energy may be returned to the spacecraft by certain elements of the solar simulator. The large parabolic mirror of a cassegrain system would return this energy. A ray tracing analysis was performed on an IBM 7090 computer to determine the amount of this energy which returns to the spacecraft for the on-axis cassegrain system in the 25-ft Space Simulator. The "spacecraft" was taken to be a polished flat circular disc. The results of this program are presented in Table 6 for three levels—corresponding to the top, middle, and bottom of the working volume as defined by the original contract specification. As can be seen, a considerable amount of this energy would be returned to the spacecraft. A simple calculation shows that the average energy flux due to the first reflection pair on a 3-ft-radius polished aluminum disc 18 ft from the floor of the test chamber would be 53% of the originally incident energy! In general, these secondary rays return to the spacecraft at considerably greater incidence angles than the primary flux, thus causing errors due to multiple reflection absorption. The geometry of the system precludes their use as a bolstering factor for the main energy stream.

Table 6. Percent of reflected solar energy returned to spacecraft* by solar simulator optics in the original cassegrain design of the JPL 25-ft Space Simulator

Spacecraft diameter, ft	Distance from floor, ft	Radial Position of Reflecting Element, ft						
		0	1	2	3	4	5	6
6	10	80.6	57.1	29.9	8.3			
	14	81.5	75.7	70.4	29.2			
	18	73.6	67.8	67.8	56.7			
8	10	81.0	80.1	47.4	16.8	16.7		
	14	82.5	76.6	71.1	38.5	27.9		
	18	78.5	72.4	68.9	74.2	67.6		
10	10	81.3	80.4	76.7	24.6	30.2	40.1	
	14	83.7	78.6	71.7	39.0	77.1	21.6	
	18	84.5	76.2	70.0	74.2	78.2	85.6	
12	10	81.8	80.5	77.0	40.3	45.4	18.7	4.4
	14	85.1	79.9	73.6	39.2	77.1	76.0	12.2
	18	91.3	84.8	73.8	74.3	78.2	76.3	79.7

*Spacecraft assumed to be polished flat circular disc of diameter shown in first column.

H. Energy Emitted by the Spacecraft and Returned to the Spacecraft by the Solar Simulator, q_8

The presence of the large parabolic mirror in a cassegrain system will be felt by the spacecraft in the infrared regime as well as that of the solar simulation spectrum. As the nature of the emission from spacecraft surfaces is probably closer to diffuse than specular, a lower percentage of this energy will strike the mirror and correspondingly less will be returned to the spacecraft. Ray tracing has shown that approximately 10 to 15% of the energy emitted by an object at the top of the test volume would be returned. This effect becomes appreciable when the upper spacecraft surfaces are black, since the reflected solar energy discussed above is decreased immensely because of the high absorptance of the black surface. These two effects (q_7 and q_8) decrease to zero for an "off-axis" cassegrain system if the test volume does not intrude into the cone whose base is defined as the plane of the mirror edge and whose height is defined as twice the focal length of the mirror as shown in Fig. 3.

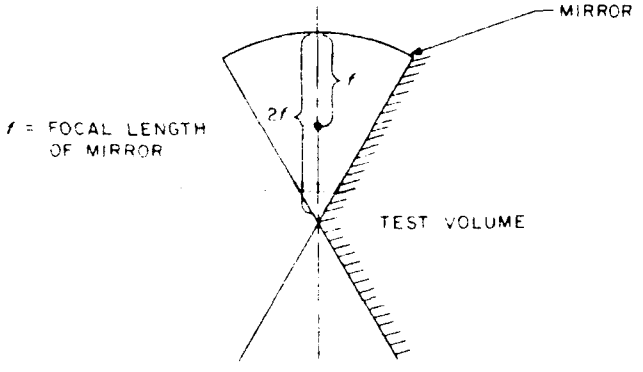

Fig. 3. Location of test volume for elimination of q_7 and q_8 errors

I. Energy Emitted by Various Optical Elements of the Solar Simulation System, q_9

The presence of various optical elements within the chamber will be felt by the spacecraft unless liquid nitrogen shrouds are provided to shield them. Mirrors will have a very small effect on a spacecraft because of their high reflectance and low emittance. An uncoated mirror at room temperature will emit 10 times more energy than a black shroud at −320 F but only 1/20th the energy of a black shroud at room temperature. In order for an uncoated mirror to emit the same amount of energy per unit area as a black shroud at −320°F, the mirror temperature must be approximately −164°F.

Transparent optical elements, however, have high emittances and could emit an appreciable amount of energy if not shielded or coated and operated at liquid nitrogen temperatures. Clearly, shielding may not be possible on systems which beam energy directly on the spacecraft, since shields would block the shorter

solar simulation wavelengths as well as the unwanted infrared. If at all possible, optical elements in the chamber should at least be operated at low temperatures in order to minimize these effects.

V. CONCLUSIONS

Specular multireflection between the spacecraft and large mirror of a cassegrain solar simulator is intolerable from a systems thermal testing standpoint. "Off center" cassegrain systems like the system presently in use in the JPL 25-ft Space Simulator not only remove the specular multireflection error, but also remove the infrared reflection error by eliminating the image of the spacecraft in the large mirror as seen from the spacecraft.

One system not mentioned above is the "boresighted" solar simulator. It may be shown by relatively simple trigonometric relations that boresighted systems of reasonable size have much higher errors resulting from sidelighting (Δq_6) than do "Sun image systems". In addition, the axial energy flux density variation is much larger and shadow malformation far more complex than in a Sun image system. These characteristics make boresighted systems look quite unattractive for thermal systems testing.

Of the errors associated with absorption of solar simulation energy, the error associated with spectral mismatch appears to be the largest. Work should definitely be continued toward the development of a permanent arc or combinations of arcs in various gases which closely approach the Johnson solar spectrum curve. An essential characteristic of any arc source is constancy of spectrum over periods of extended operation or numerous start-ups and shut-downs. A reliable scheme for monitoring the solar simulator spectral distribution during thermal systems tests should also be developed.

Improvement of the degree of decollimation of the solar source will reduce the errors associated with absorption of direct and reflected solar energy, shadow blurring, side lighting, and variation of uniformity of incident solar energy. In some rare cases, it may be possible to circumvent these errors by designing the spacecraft with solar simulator testing problems in mind. However, this generally will not be possible. Since analytical techniques cannot be used to determine all of the errors resulting from decollimation, it seems necessary to approximate the solar collimation angle (32 min as accurately as is possible.

The information contained in the previous tables and discussion may be summarized in Tables 7, 8, and 9. Following is a summary of subscripts used in Tables 7, 8, and 9:

1 = electrical power dissipation

2 = direct solar energy absorbed

3 = reflected solar energy absorbed

4 = infrared energy absorbed from other spacecraft nodes

5 = conduction input from other spacecraft nodes

6 = energy absorbed due to sidelighting

7 = solar energy absorbed after reflection by spacecraft to optics and return

8 = energy emitted by spacecraft, returned to spacecraft by optics, and reabsorbed

9 = energy emitted by optics and absorbed by spacecraft

Table 7. Summation of heat inputs (in watts) based on space conditions

	q_1	q_2	q_3	q_4	q_5	$\Sigma\, q_n$
Electronic assembly	17.6	9.7	1.5	0.6	1.5	30.9
Science package	0.6	13.2	2.9	0.6	0.6	17.9
Structural element (leg)	0.0	2.9	1.5	0.6	1.5	6.5

Table 8. Breakdown of $\setminus q_2$

	$\setminus q_{2\ \text{spectral}}$	$\setminus q_{2\ \text{decollimation}}$			Total, %	$\setminus q_2$, w
	Spectral mismatch, %	Vertical nonuniformity, %	Axial nonuniformity, %	Shadow malformation, %		
Electronic assembly	8.5 (gold)	5	5	0	18.5	1.8
Science package	8.5 (gold)	5	5	15	33.5	4.4
Structural element	8.5 (gold)	5	5	15	33.5	0.97

Table 9. Total $\setminus q_n$ (in watts) and summation of Equation (6)

	$\setminus q_1$	$\setminus q_2$	$\setminus q_3$	$\setminus q_{4\ \&\ 5}$	$\setminus q_6$	$\setminus q_{7,\ 8,\ 9}$	$\Sigma \setminus q_n$	$\dfrac{\Sigma \setminus q_n}{\Sigma q_n}$
Electronic assembly	0.0	1.8	1.5	0.0	1.3	Designed out of chamber	4.6	0.14
Science package	0.0	4.4	2.9	0.0	1.0		8.3	0.44
Structural element	0.0	0.97	1.5	0.0	1.0		3.4	0.53

A comparison of the values in the last column of Table 9 with the summation of Eq. (5) indicates that a thermal test with solar simulation under the conditions stated here would provide meaningful data for major electronic assemblies. The data from smaller elements of the spacecraft such as structural elements and science packages would probably be less significant. The use of special paint patterns or nonflight modifications (heaters to make up for lack of solar energy or shields to guard against too much solar input) would aid science packages or structural elements in operating near flight cruise temperatures. However, careful test data analysis using well defined system operating parameters is necessary in order to meaningfully interpret the test results.

APPENDIX A

Revision of Tables Reflecting *Ranger* Block III Design

The tables in the main body of this memorandum were based principally on the thermal design characteristics of the *Ranger* Block II spacecraft. These tables have been revised (Tables A1 – A9) to reflect the thermal design characteristics of the *Ranger* Block III spacecraft. Where applicable, new data on solar absorptances, etc., have been included.

The average unknown in emittance for *Ranger* Block III electronic chassis is 3%. Tolerance imposed on flight cruise temperatures is ± 40 F about a nominal 85 F. Recalculated analytical value of $\Sigma \alpha q_a / \Sigma q_a$ (Eq. 5):

$$\frac{\Sigma \alpha q_a}{\Sigma q_a} = 0.03 + 4\left(\frac{40}{545}\right) = 0.26 \qquad (A5)$$

Table A1. Absolute emittance and relative uncertainty of typical spacecraft surfaces

Material	Absolute emittance	Relative uncertainty, %
Black paint	0.90 ± 0.02	2
White paint (PV 100)	0.85 ± 0.02	2
White paint (JW 40)	0.78 ± 0.02	3
Aluminum paint	0.30 ± 0.03	10
Polished aluminum (commercial polish)	0.045 ± 0.005	11
Gold plate	0.035 ± 0.005	14

Table A2. Average power dissipations for three spacecraft elements, q_1

Object	Power dissipation, w
Major electronic assembly	14.2 to 31.6
Science package	0.1 to 1.0
Structure	0

Table A3. Solar energy absorbed by three spacecraft elements, q_2

Object	Energy absorbed, w
Major electronic assembly (Average of 5 *Ranger* Block III chassis)	27.7
Science assembly	5.0 to 20
Structure (*Ranger* leg)	2.3

Table A4. Deviation of absorptance in mercury-xenon spectrum from solar absorptance

See Table B1 (Appendix B)

Table A5. Sidelighting energy absorbed by surfaces parallel to Sun-probe line for three values of solar simulator decollimation half-angle, watts

Object	Area, ft^2	2 deg	4 deg	6 deg
Electronic assembly	2.0	0.62	1.25	1.88
Science box	1.5	0.36	0.72	1.08
Leg	1.4	0.27	0.54	0.81

Note: The values of energy absorbed in this table differ from those in Table 5 on page 13 owing to the use of absorptance values obtained in the JPL 25-ft Space Simulator (Table B1) and the surface coatings used in the *Ranger* Block III thermal design.

Table A6. Percent of reflected solar energy returned to spacecraft by solar simulator optics in the original cassegrain design of the JPL 25-ft Space Simulator

Same as Table 6, page 14.

Table A7. Summation of heat inputs (in watts) based on space conditions

	q_1	q_2	q_3	q_4	q_5	Σq_n
Electronic assembly	27.0	27.7	2.0	1.0	2.0	60.0
Science package	0.6	13.2	2.9	0.6	0.6	17.9
Structure	0.0	2.9	1.5	0.6	1.5	6.5

Table A8. Breakdown of Δq_2

	$\Delta q_{2\ spectral}$	$\Delta q_{2\ decollimation}$				
	Spectral mismatch, %	Vertical nonuniformity, %	Axial nonuniformity, %	Shadow malformation, %	Total, %	Δq_2, watts
Electronic assembly	0 (black)	5	5	0	10	2.8
Science package	19 (gold)	5	5	15	44	5.8
Structure	16 (aluminum)	5	5	15	41	1.2

Table A9. Total Δq (in watts) and summation of Equation (6)

	Δq_1	Δq_2	Δq_3	$\Delta q_{4\ \&\ 5}$	Δq_6	$\Delta q_{7,\ 8,\ 9}$	Δq_n	$\frac{\Sigma \Delta q_n}{\Sigma q_n}$
Electronic assembly	0	2.8	2.0	0	0.6	Designed out of chamber	5.4	0.09
Science package	0	5.8	2.9	0	0.4		9.1	0.51
Structure	0	1.2	1.5	0	0.3		3.0	0.46

APPENDIX B
Some Comments on Recent Thermal Tests in the JPL 25-ft Space Simulator

Since the original work was done on this report, four thermal tests have been carried out in the JPL 25-ft Space Simulator by the *Ranger* thermal groups of JPL and RCA. The objects tested were a thermal model of the RCA television subsystem, a complete thermal model of the *Ranger* Block III spacecraft (tested twice), and the *Ranger* Block III proof test model. Some of the effects discussed in the preceding pages were encountered during these tests and are discussed below.

Decollimation of the solar simulation source resulted in probably the most significant problem encountered during this series of tests. Two preliminary investigations into the effect of decollimation on the RCA subsystem were performed before the RCA Temperature Control Model (TCM) was suspended in the simulator. A special large-aperture camera was used to photograph the solar simulator light source to obtain an estimate of the degree of decollimation of the source. In addition, a test fixture simulating the fin configuration of the TCM was examined under the solar simulation light beam. With the data obtained from these investigations, together with incident energy flux mapping data obtained from the TCM in the light beam, it was hoped to determine the amount of energy reflected from the conical skin of the RCA TCM onto the annular fins. When the TCM was illuminated by the solar simulator, approximately 40% of the polished aluminum skin was partially illuminated by the solar source. In space, the fins would completely shade the skin. The thermal vacuum test of the RCA TCM resulted in an average equilibrium temperature approximately 40 F higher than that predicted for flight (63 F). Even with the data obtained from the two preliminary investigations and the energy flux mapping of the RCA TCM itself, 16% of the energy absorbed by the subsystem in the thermal vacuum test could not be accounted for.

After analysis of the RCA TCM test results, the following recommendations were made:

1. Eliminate directly incident decollimated light from striking the skin of the TCM.
2. Improve the instrumentation used for determination of energy flux density.

These recommendations were implemented for the first test of the complete *Ranger* Block III TCM (JPL bus with RCA subsystem attached). Fin extensions were added to the RCA subsystem solar absorbing fins, increasing the effective width of these fins. These extensions were attached so as not to add to the energy absorbed by the fins themselves and were trimmed to a width which would shade the polished aluminum skin

of the subsystem from directly incident energy. A thermopile was used in this test to monitor solar simulation flux density, replacing the solar cell used in the first test of the RCA TCM. Although the average equilibrium temperature of the RCA subsystem under solar simulation in this test was considerably lower than the predicted flight temperature, 100% of the energy input to the subsystem could be accounted for. This was a significant improvement over the results of the first RCA TCM test. The lower-than-flight temperature in this test resulted from partial blockage of directly incident solar energy on the TCM fins and, in some locations, partial shadowing of the fin by the ring on the fin above.

When the solar simulator lights were initially turned on for the complete TCM, the white surfaces on the fronts of the electronic chassis were illuminated due to decollimation of the solar simulation source. Based on the difficulties encountered with the RCA TCM in the first test, shading strips or "eyebrows" were added to the tops of the cases to eliminate illumination of the vertical case surfaces. The energy flux on the fronts of the cases was reduced considerably by these "eyebrows."

Values of absorptance in the mercury-xenon spectrum of the 25-ft Space Simulator were experimentally evaluated through the use of a "button box" developed at JPL (Ref. 3). The mercury-xenon absorptances were used in evaluating the test data obtained in the TCM tests and PTM test. The absorptance values obtained, together with their respective solar absorptances (calculated from the Johnson curve), are listed in Table B1. The mercury-xenon absorptances are thought to be accurate to ± 10%.

Table B1. Comparison of measured Hg-Xe absorptances in JPL 25-ft Space Simulator with calculated solar absorptances for several spacecraft surface treatments

Surface	Solar α_s	Hg-Xe α_s	Percent Error
Polished gold	0.22	0.263	- 19.5
Polished aluminum	0.185	0.214	- 15.7
Cat-a-lac black paint	0.96	0.962	- 0.2
JW-40 white paint	0.225	0.387	- 72.0
RCA No. 1 (white with 0.7% black)	0.37	0.43	- 16.2
RCA No. 2 (white with 3.2% black)	0.55	0.58	- 5.5
RCA No. 3 (white with 12.9% black)	0.76	0.82	+ 7.9
RCA No. 4 (PV-100 white)	0.22	0.31	+ 41.0

Energy flux mapping of the spacecraft surfaces was performed before each thermal test. The purpose of the mapping was to furnish data on directly incident and reflected solar energy for the various spacecraft surfaces. As stated previously, this mapping did not eliminate the errors due to a warped spacecraft temperature field. However, it did facilitate the calculation of solar energy absorbed on various portions of the spacecraft in the analysis of test data. Unfortunately, the accuracy of these calculations is limited by the accuracy of the mapping data, which is estimated to be ±5 watts ft^{-2}.

More detailed descriptions of these tests may be found in Refs. 4 – 7.

REFERENCES

1. Johnson, F. S., "The Solar Constant," *Journal of Meteorology*, Vol. II, No. 6, December 1954, pp. 431-439.

2. Personal communication from H. N. Riise, Jet Propulsion Laboratory.

3. Personal correspondence with D. W. Lewis, Jet Propulsion Laboratory.

4. Lerner, M., "*Ranger* Block III Temperature Control Report on Thermal Control Model Tests (Phase I) in 25-ft Space Simulator With Use of Solar Lights," JPL interoffice document, August 1, 1963.

5. Lerner, M., "*Ranger* Block III Temperature Control Report On Thermal Control Model Tests (Phase II) in 25-ft Space Simulator," JPL interoffice document, August 30, 1963.

6. Lerner, M., "*Ranger* Block III Temperature Control Report on Proof Test Model Tests," JPL interoffice document, November 11, 1963.

7. *Ranger TV Subsystem, Block III*, Thirteenth Bimonthly Progress Report, Radio Corporation of America, October 8, 1963.